Three-dimensional structure of a human class II histocompatibility molecule complexed with superantigen

Theodore S. Jardetzky, Jerry H. Brown*†, Joan C. Gorga‡, Lawrence J. Stern*, Robert G. Urban, Young-in Chi§, Cynthia Stauffacher§, Jack L. Strominger & Don C. Wiley*‖

Department of Biochemistry and Molecular Biology, * Howard Hughes Medical Institute, Harvard University, 7 Divinity Avenue, Cambridge, Massachusetts 02138, USA
† Rosenstiel Research Center, Brandeis University, 415 South Street, Waltham, Massachusetts 02154, USA
‡ Department of Pediatrics, Children's Hospital of Pittsburgh, 6130 Rangos Research Building, 3705 Fifth Avenue, Pittsburgh, Pennsylvania 15213, USA
§ Department of Biology, Purdue University, West Lafayette, Indiana 47907, USA

The structure of a bacterial superantigen, *Staphylococcus aureus* enterotoxin B, bound to a human class II histocompatibility complex molecule (HLA-DR1) has been determined by X-ray crystallography. The superantigen binds as an intact protein outside the conventional peptide antigen-binding site of the class II major histocompatibility complex (MHC) molecule. No large conformational changes occur upon complex formation in either the DR1 or the enterotoxin B molecules. The structure of the complex helps explain how different class II molecules and superantigens associate and suggests a model for ternary complex formation with the T-cell antigen receptor (TCR), in which unconventional TCR–MHC contacts are possible.

SUPERANTIGENS comprise a class of disease-associated, immunostimulatory molecules that bind class II MHC molecules and stimulate large numbers of T cells[1,2]. Members of the superantigen family include toxins from *S. aureus* and other bacteria[3], as well as viral superantigens from mouse mammary tumour virus (MMTV)[4]. The *S. aureus* toxins are associated with food poisoning and toxic-shock syndrome, and the MMTV superantigen plays a critical role in viral transmission. The toxicity of bacterial superantigens is thought to be mediated by their potent T-cell-stimulating activities[5], leading to lymphokine release[6], respiratory distress and shock. Superantigens have also been implicated in rabies, rheumatoid arthritis, and mouse and human AIDS[7].

The mechanism by which superantigens stimulate T cells differs from that of normal antigens. Conventional T-cell antigens are short proteolytic peptides from foreign proteins, bound in the peptide-binding groove of class I or class II MHC molecules[8]. The structures of both class I and class II MHC molecules[9–11] demonstrate that these bound peptides become an integral part of the MHC protein surface, which is displayed by antigen-presenting cells to specific T cells, generating an immune response. In contrast, bacterial superantigen activity is abolished by proteolysis and it is the intact superantigen protein that interacts with class II MHC molecules outside the peptide-binding groove[12,13] in order to stimulate T cells.

The interaction of conventional peptide antigens and superantigens with the T-cell antigen receptor (TCR) also differs. TCR molecules are structurally related to antibody molecules, with hypervariable regions forming a combining site for a specific peptide–MHC combination[12]. Superantigens bypass this specificity-determining region of the TCR, and interact with a surface of the TCR predicted to lie outside the antigen-combining site on the variable β-chain (Vβ) domain[14–18]. This ability of superantigens to interact with both MHC and TCR molecules outside their normal antigen-specific sites leads to the stimulation of many more T cells than observed with normal peptide antigens.

To understand better the molecular basis of the pathological effects of superantigens, we have determined the structure of a bacterial superantigen, *S. aureus* enterotoxin B (SEB), bound to a human class II MHC molecule, HLA-DR1, by X-ray crystallography. SEB binds outside the MHC peptide-binding site, with the N-terminal domain of SEB interacting with the DR1 α1 domain. No large conformational changes are observed in either the class II molecule[11] or the SEB molecule[19] upon complex formation. SEB residues that affect the interaction with T-cell receptors are positioned to the side and above the DR1 peptide-binding site of the class II molecule, suggesting a model for the interaction of superantigen–MHC complexes with TCR, where normal TCR–MHC interactions are blocked.

Structure determination

The structure of the DR1–SEB complex was determined using the data sets listed in Table 1, from two different DR1–SEB crystal forms. Initial electron density maps were generated using SIR/anomalous phases for crystal form I and improved by averaging with maps derived from HLA-DR1 crystals as described[11]. The initial model of the DR1 molecule was improved by cycles of building and refinement and a partial model for the SEB was built. A low-resolution data set of crystal form II (Table 1) was solved by molecular replacement with the partial model of the complex, and iterative non-crystallographic four-fold symmetry averaging was used (Fig. 1*a*) to obtain a polyalanine trace for 190 residues of the SEB molecule at low resolution. This model was used to calculate higher-resolution electron-density omit maps, followed by iterative non-crystallographic two-fold symmetry averaging, with data from crystal form I, and improved by further cycles of building and refinement (Fig. 1*b*).

‖ To whom correspondence should be addressed.

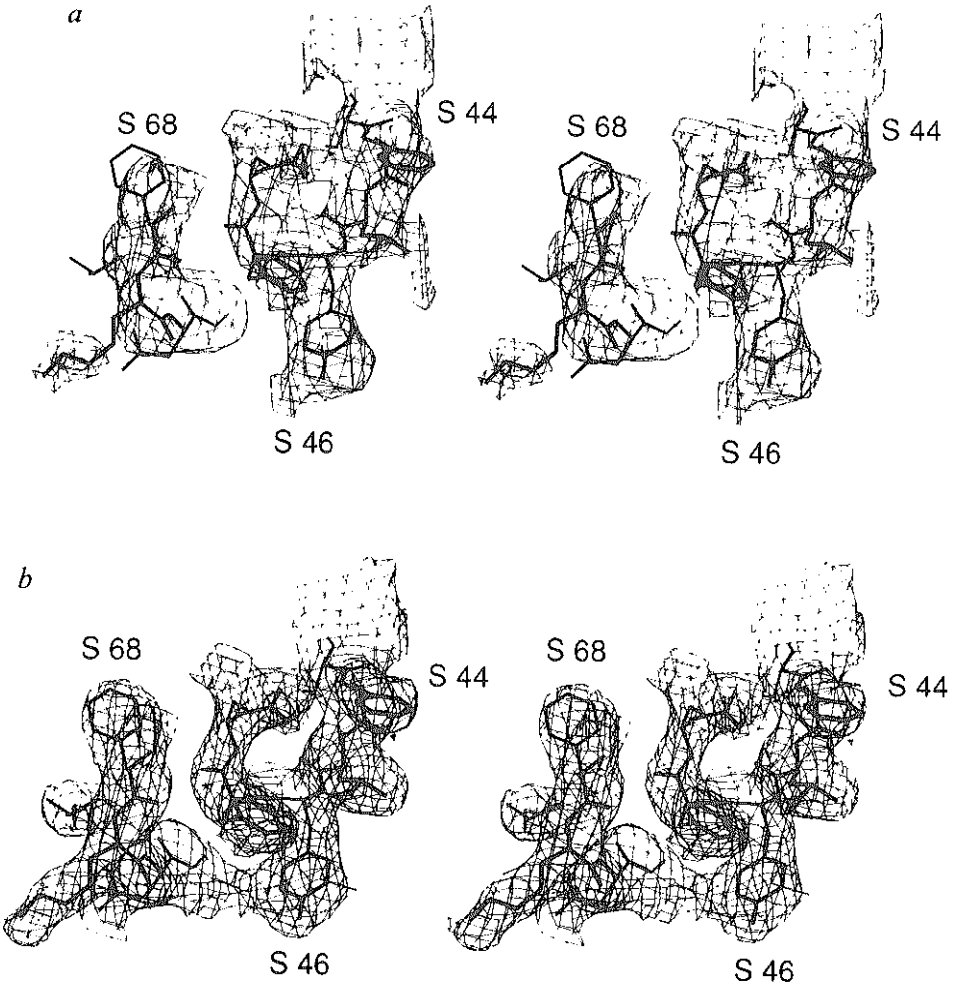

FIG. 1 Electron density maps and temperature factors for the DR1–SEB complex. SEB electron density maps at the DR1–SEB interface. *a*, 15.0–4.3 Å $|2F_o - F_{calc}|$ map generated by 4-fold iterative averaging between crystal form I and form II. *b*, A current 2-fold averaged $|2F_o - F_{calc}|$ omit map at 2.7 Å resolution, calculated using current model phases and data from crystal form I, omitting the atoms shown. Both maps are contoured at 1.0σ with a cover radius of 1.5 Å around the atoms shown. *c* and *d*, Top and side views (respectively) of the DR1–SEB complex showing the radial increase in temperature factor. Two DR1–SEB complexes are found in the asymmetric unit as shown. The current model is coloured by temperature factor (atomic *B*-factor), with blue representing Cα *B*-factor values less than 25 Å^2 and red representing *B*-factor values greater than 100 Å^2 (see Table 1 for average SEB *B*-factors). Note the increase in *B*-factor as a function of distance from the DR1–SEB interface, and the correspondence with loops in the DR1 structure. The high-temperature factors may be due to SEB disorder within the crystal lattice. One SEB makes no contacts with other symmetry-related molecules in the lattice, whereas the other SEB molecule has only few crystal contacts in regions of the C-terminal domain that may not be accurately modelled. The DR1 molecules form crystal contacts in all lattice directions and may provide the predominant stabilization of the crystal lattice. The high-temperature factors may therefore also reflect a lower SEB occupancy within the lattice. Refinement of SEB occupancy before *B* refinement typically provides an improvement in R_{free} of 0.3–0.5%. Further experiments are necessary to resolve these possibilities.

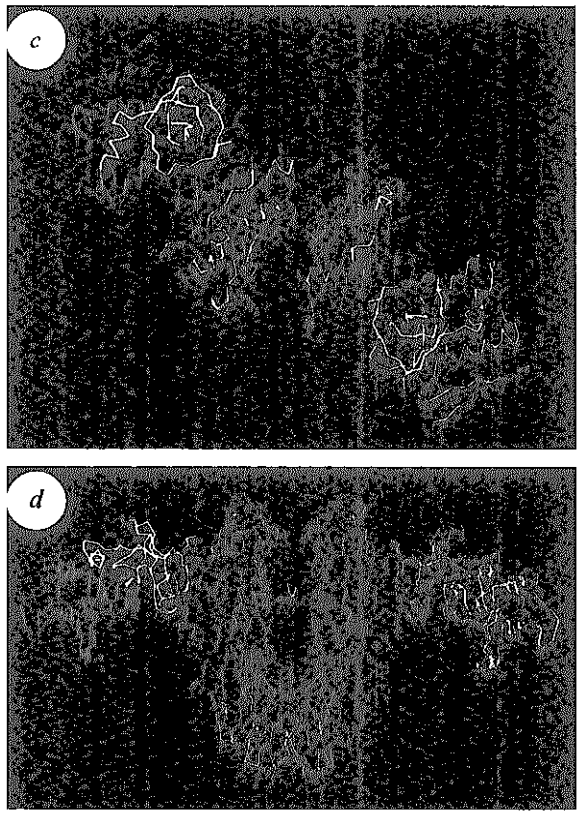

The structure of the complex shows a gradient of disorder of the SEB molecules, extending radially out from the DR1–SEB interface (Fig. 1*c*, *d*). This has two consequences. First, five surface loops of the SEB molecules show no interpretable electron density, presumably because of the higher basal level of SEB disorder. Second, the SEB C-terminal domain shows generally weaker electron density, with stunted or absent side-chain density. The N-terminal domain of the SEB molecule, which forms most of the contacts to DR1 (Fig. 1*b*; and shown in yellow in Fig. 2*a*) is, however, the best ordered region of the SEB structure. The disorder evident in the structure does not affect either our major conclusions as to how SEB binds to class II MHC molecules or the implications for TCR interactions.

Overview of DR1–SEB complex formation

Figure 2 shows top and stereo views of the DR1–SEB complex. SEB only contacts residues of the α1 domain of DR1, interacting with amino acids from the first and third turns of the β-sheet and from the N-terminal region of the α-helix. These residues form a deep, concave surface to one side of the peptide-binding site of DR1 (Fig. 3*c*), in agreement with mutational studies mapping the MHC–SEB interaction[13]. The potential influence of α-chain polymorphisms in the binding of SEB to other human and mouse class II molecules is discussed later. SEB does not interact

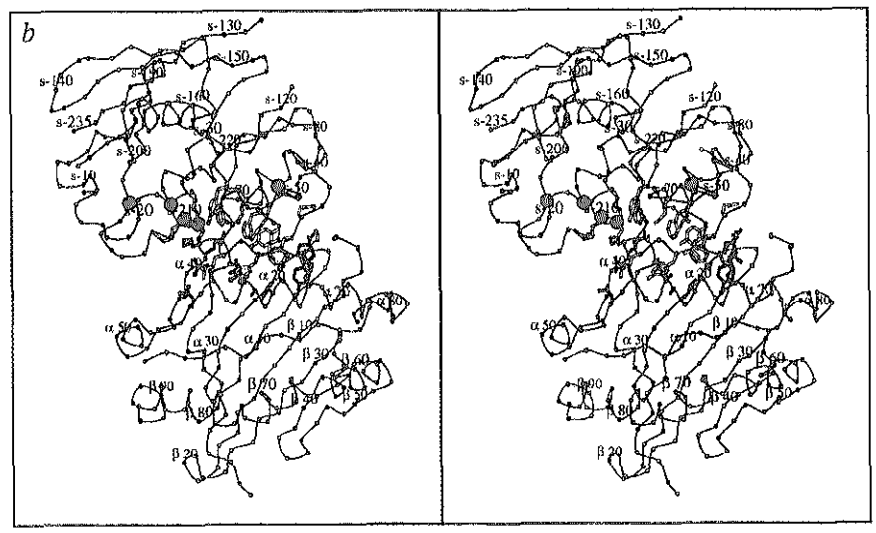

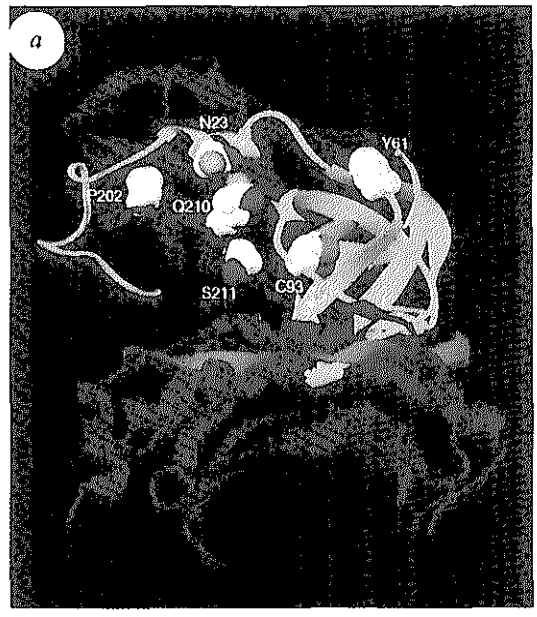

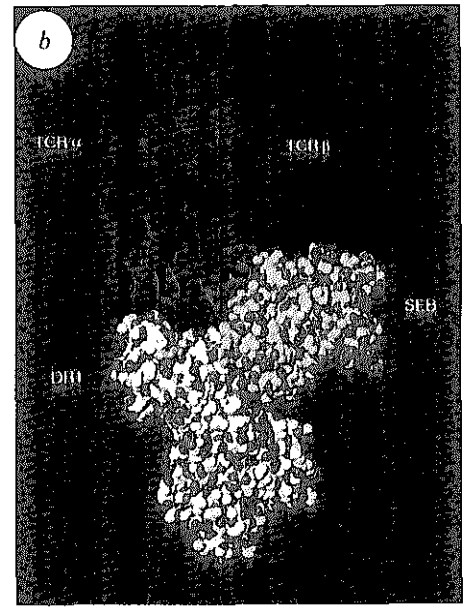

FIG. 2 Overview of the complex between HLA-DR1 and SEB. *a*, Top view, HLA-DR1 α1 and β1 domains are shown in blue; α2 and β2 domains are not shown. N-terminal residues of SEB 2–121 are in yellow, and C-terminal residues 127–235 of SEB are in red; the peptide is shown in pink. The peptide conformation is based on fitting a polyalanine chain into the observed electron density corresponding to a mixture of self-peptides bound to the HLA-DR1 molecule. *b*, Cα trace of the complex (DR1 α2 and β2 not shown), showing all side chains involved in the DR1–SEB interface. SEB interface residues are in yellow; DR1 interface residues are in dark blue. Red spheres mark the SEB and SEA residues implicated in TCR interactions[2,24,41–43].

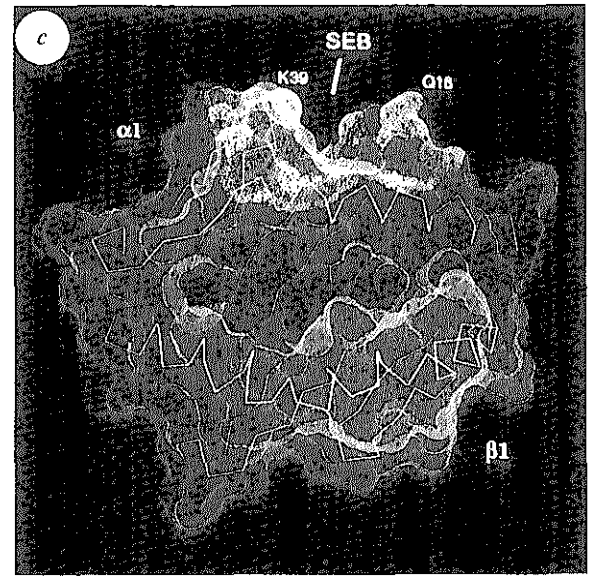

FIG. 3 Location of superantigen residues involved in TCR interactions and a model of ternary complex formation between DR1, SEB and TCR. *a*, Residues in SEB (N23, Y61, C93–C113; N60 not shown) and SEA (in SEA: G200, S206, N207; in SEB P202, Q210, S211) that have been implicated in TCR interactions by mutagenesis[2,24,41–43]. DR1 α1 and β1 domains are blue (DR1 α2 and β2 domains are not shown), SEB is yellow (N-terminal residues) and red (C-terminal residues), and peptide is pink. CPK representation is white for carbon atoms, red for oxygen, blue for nitrogen, and green for sulphur. *b*, Hypothetical model of ternary complex formation of DR1 and SEB with TCR. An immunoglobulin Fab fragment model of the TCR α-chain in blue, β-chain in red. Hypervariable regions of TCR (CDR1, CDR2 and CDR3) are shown in yellow, and the HV4 loop and *B* strand of the Vβ domain are shown in white. DR1 carbon atoms are white, SEB carbon atoms are yellow, peptide carbon atoms are magenta. The view is looking down the DR1 peptide-binding site, with the DR1 β-chain to the left and the α-chain to the right. The TCR is positioned so that the SEB residues shown in *a* can interact with the white HV4 loop. *c*, Top view of the class II molecule, showing the region of the α1 domain buried by complex formation with SEB. Surface of the DR1 molecule shown in magenta outside the SEB interaction area. Blue, hydrophobic surface buried by SEB; yellow, polar surface buried by SEB.

with class I MHC molecules and this region differs in class I and class II MHC structures[11]. Good peptide density is observed in the peptide-binding site, corresponding to a mixture of self-peptides, and has been modelled as polyalanine (Fig. 2). SEB does not interact directly with the peptide and the peptide conformation is very similar to that observed for a single peptide–DR1 complex[20].

Residues from the SEB molecule that interact with DR1 derive predominantly from the smaller N-terminal β-barrel domain of the SEB molecule, although three residues from the C-terminal helix 5 (residues 210–217) also contact the DR1 molecule. Helix 5 is actually more closely associated with the N-terminal domain than with the C-terminal domain (Fig. 2*b*). The SEB residues most central to the interface lie in a turn between strands 1

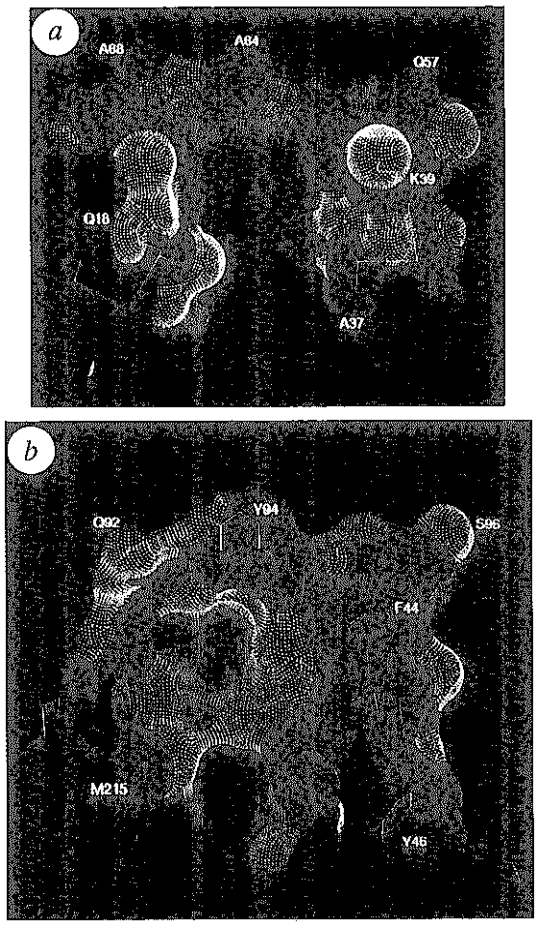

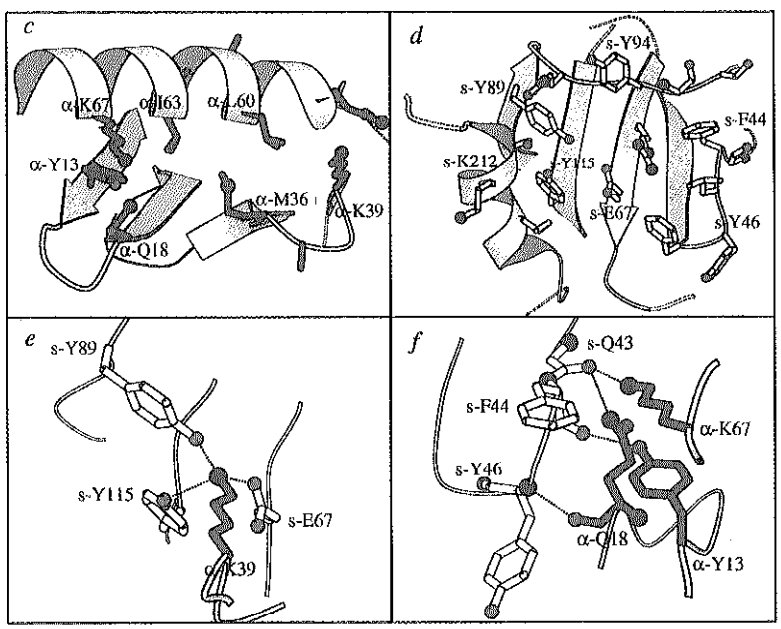

FIG. 4 The DR1–SEB binding interface. *a*, Surface view of the DR1 residues involved in binding to SEB. Yellow, polar atoms at surface; blue, hydrophobic atoms at surface. *b*, Surface view of the SEB residues involve in binding, same colour scheme as in *a*. *c*, DR1 residues involved complex formation, side view. DR1 residues are shown with blue bonds. Red, green and dark blue spheres represent oxygen, sulphur and nitrogen atoms, respectively. *d*, SEB residues involved in complex formation. SEB residues are shown with yellow bonds and atoms coloured as in *c*. *e*, Salt bridge formed between DR1 α-chain residue lysine 39 and SEB glutamic acid 67, with SEB tyrosines 89 and 115 forming hydrogen bonds. *f*, Potential hydrogen bonds formed between residues of the DR1 molecule and the main chain of residues 43–46 of the SEB molecule. Surfaces generated with MS[23] using a probe radius of 1.4 Å, and displayed in O[64]; *c*–*f* generated with Molscript[65]. Surfaces areas quoted in the text were calculated with the default atomic radii used by the program Access[22] and a probe radius of 1.4 Å.

(residues 33–39) and 2 (residues 48–52) and along strand 3 (residues 63–68). In addition, a stretch of residues in the SEB disulphide loop (residues 92–96) runs above the binding interface parallel to the DR1 α1 α-helix. The C-terminal domain of the SEB molecule is oriented up and away from the class II molecule, consistent with the observation that N-terminal constructs containing residues 1–138 of the SEB molecule bind class II MHC molecules and retain partial activity[21].

Description of the Interface

Figure 2*b* shows a stereo view of the DR1 and SEB residues involved in complex formation. The interface is comparable in size to antigen–antibody interfaces, burying 780 Å^2 and 760 Å^2 of the DR1 and SEB solvent-accessible[22] surfaces respectively. Twenty-one residues of the DR1 molecule and nineteen residues from the SEB molecule are involved in complex formation.

A topological view of the binding interface shows a dramatic division of the complementary surfaces of the DR1 and SEB molecules. Figure 4*a*, *b* shows the molecular surfaces[23] of the DR1 and SEB molecules respectively, which are buried upon formation of the complex (coloured blue for non-polar atoms and yellow for polar atoms). Each binding surface is divided into two regions, one predominantly hydrophobic and one predominantly polar.

The hydrophobic region of the interface consists of a ridge of non-polar residues (F44, L45 and F47 (single-letter amino-acid code with residue number)) protruding from the loop between strands 1 and 2 of the SEB molecule (Fig. 4*b*, blue; and Fig. 4*d*), which fits into a predominantly hydrophobic depression on the DR1 molecule formed by residues of loops 1 and 3 and the α-helix of the α-chain (Fig. 4*a*, blue; Figs 3*c* and 4*c*). DR1 residues that contribute to this interaction include hydrophobic residues Y13, M36, A37, L60, I63 and A64, as well as the aliphatic portions of more polar residues such as Q18 (Fig. 4*c*). Mutations of residues F44 and L45 in the SEB molecule disrupt binding to class II MHC molecules[24].

The polar region of the binding interface is more apparent on the SEB interaction surface, to the left of the hydrophobic ridge (Fig. 4*b*). This polar pocket on the SEB surface is complemented by a protrusion from loop 3 of the DR1 molecule formed by lysine 39 (Fig. 4*a*, *e*). This lysine forms a completely buried salt bridge with glutamic acid at position 67 of SEB, surrounded by hydrogen bonds from SEB Y89 and Y115 (Fig. 4*e*). The mutation of lysine 39 to alanine in the DR1 molecule reduces SEB binding[40].

Three other residues of HLA-DR1 (Y13, Q18 and K67) are potentially involved in hydrogen bonds to the main chain of SEB residues 43–46 (Fig. 4*f*) and may be important in positioning the hydrophobic residues of the SEB molecule between the DR1 loops. As these residues vary between class II isotypes (Fig. 5), they may play a part in determining differences in the overall binding affinity.

In addition, SEB disulphide loop residues 92–96 contact the α1-domain α-helix of the DR1 molecule along the upper face of the interaction region (Fig. 4*d*). In particular, SEB Y94 forms an extensive set of hydrophobic interactions with DR1 residues 60 and 61, whereas SEB S96 contacts DR1 residues 64, 67 and 68. Although these SEB residues do not bind into distinct pockets on the DR1 molecule, they have important implications for the accessibility of DR1 residues to TCR interactions (see below).

Two SEB residues (14 and 17) have been implicated in MHC binding[24], but are not directly involved in the DR1–SEB interface and may have an indirect effect on MHC binding. This conclusion is supported by the observation that deletion of SEB residues 1–30 does not abrogate the ability of SEB to stimulate polyclonal T cells[21].

Other class II molecules and SEB

The binding affinity of SEB varies between different class II MHC molecules. The ability of SEB to bind many different DR allotypes[25] can be explained by its exclusive interaction with the DR1 α-chain, which is conserved in all DR molecules. Binding to other class II isotypes is weaker than binding to DR[26–29] in the order DR > DQ > DP[25,29], whereas for mouse alleles I-E binds SEB better than I-A[29], but both bind more weakly than DR.

Figure 5*a* shows a plot of the surface of the DR1 molecule that is buried by the interaction with SEB, along with the corresponding residues that are found in other human (DP/DQ) and mouse (I-A/I-E) alleles. For the human class II isotypes DP and DQ, about 50% of the residues in the DR1–SEB interface are conserved, although the subset of these residues differs between DP and DQ. Lysine 39 is found in all three isotypes, indicating that a salt bridge with E67 of SEB could be formed (Fig. 4*e*). Many of the residues that form the hydrophobic portion of the interaction surface (Fig. 4*c*, and shown in blue in Fig. 4*a*) are conserved (L60, A64) or conservatively substituted (M36 to L, I63 to I or M).

Although a number of residue differences could account for a lower binding affinity for DQ and DP, relative to DR, the substitution of Q18 to proline in both DQ and DP is particularly central to the DR1–SEB interface. Proline would disrupt one hydrogen bond (Fig. 4*e*), and would potentially alter the conformation of the other residues in this loop. DP molecules have additional mutations in residues in this region (Y13 to valine and K67 to asparagine) that form one side of the SEB binding site (Figs 3*c* and 4*a*, *b*), which could further destabilize the interaction with SEB molecules.

In the case of the mouse class II molecules, 12 of 17 residues are conserved in I-E molecules and 10 of 17 in I-A molecules. I-E molecules have a lysine-to-serine mutation at position 39, which would abolish the salt bridge with SEB (Figs 4*e* and 5*a*). Serine may partially compensate for the lost salt-bridge interaction. Further mutational studies are needed to define the function of different amino acids at the interface.

Other superantigens and class II molecules

Although the sequence similarity of different *S. aureus* toxins with SEB ranges from 40 to 90%, there is evidence for distinct MHC binding sites for different toxins[28,30,31]. Binding of *S. aureus* enterotoxin A (SEA) has been mapped to the MHC class II β1 domain[32,33]; binding of toxic-shock-syndrome toxin TSST-1 has been shown to be sensitive to both α1 and β1 domains[34–36]. A comparison of the SEB residues involved in binding to DR1 with the corresponding residues in SEA and TSST-1 provides some insight into the functional data available for these toxins.

Figure 5*b* shows a plot of the buried surface area of the SEB residues involved in binding DR1, with the corresponding residues from other *S. aureus* toxins. Of the DR1–SEB interactions described above, a number of central residues are conserved or conservatively substituted in SEA, including F44, L45, D67, Y89 and Y115. The conservation of these residues suggests that SEA may bind to class II molecules in a similar way to SEB. Substitution of the amino acids corresponding to SEB residues F44 and L45 in SEA (F47, L48) reduces its T-cell-stimulatory activity[37] and substitution of SEA L48 reduces MHC binding but does not abolish it (J. Kappler, personal communication). Other interactions discussed below may contribute to additional SEA binding.

Figure 5*b* shows that the major features of the SEB-binding interface are absent in TSST-1, based on a structural alignment of the two proteins[38,39]. These changes include the loss of the hydrophobic ridge (F44 to S) and the residues that interact with DR1 K39 (SEB E67 to I, Y89 to T, Y115 to I). Mutation of α-chain residues M36 to I, or K39 to S, abolishes TSST-1 binding to HLA-DR7 (ref. 35). Both of these residues are directly involved in the DR1–SEB binding interface (Fig. 4) and mutation of K39 to A disrupts SEB binding as well as TSST-1

binding[40]. This indicates that although SEB and TSST-1 are sensitive to mutations in the same region of the class II α-chain, their specific interactions may be substantially different.

Superantigen residues interacting with TCR

Some mutations in the SEB molecule affect T-cell stimulation, but not class II binding, suggesting specific contacts with the TCR[24]. These residues are shown in Figure 3*a*, together with residues that determine Vβ specificity between enterotoxins SEA and SEE[2,41,42]. The SEA residues are in the C-terminal domain of the superantigen structure, in a loop between strand 9 and helix 5 of SEB. Mutation of the cysteine residues involved in the disulphide bond in SEA[43] and SEB[24] also prevents T-cell stimulation. All of these residues line a region between the two domains of the superantigen, defining a potential TCR-binding site that is located above and to one side of the MHC peptide-binding groove (Fig. 3*a*).

Implications for ternary complex with TCR

The hypervariable region 4 (HV4) of the Vβ domain of the TCR is important for superantigen interactions[14–18]. In a hypothetical model of the TCR[44], this region lies on an exposed face of the Vβ domain (shown in white in Fig. 3*b*). Direct binding studies with a soluble TCR β-chain[45] indicate that these interactions may be sufficient for formation of an MHC–superantigen–TCR complex.

The juxtaposition of the HV4 region of the TCR with the superantigen residues involved in TCR interactions leads to a model with interesting implications for the formation of the ternary complex between MHC, SEB and TCR (Fig. 3*b*). The complementarity-determining regions (CDRs) of the TCR are oriented over the MHC peptide-binding site, with the Vβ domain bound to SEB and the Vα domain above the class II β1 domain. This model is consistent with a role for both the TCR α-chain and MHC polymorphism in modulating super-

TABLE 1 Data collection and refinement statistics

Data	Cell dimensions (Å)	Resolution (Å)	R_{sym} (%)*	Completeness (%)
Crystal form I, space group $P2_12_12_1$				
Native	95.0 × 114.7 × 149.8	30.0–2.7	5.7	86
Synchrotron		2.8–2.7	32.1	87
Crystal form II, space group $P2_12_12_1$				
Native	95.8 × 127.0 × 183.8	30.0–4.35	11.4	82
GX-13		4.69–4.35	31.0	63

Refinement statistics						
Resolution (Å)	No. of reflections (working set)	No. of atoms†	R.m.s. bonds (Å)‡	R.m.s. angles‡	R_{cryst} (%)§	R_{free} (%)‖
6.0–2.7	31,557	9,400	0.017	2.16	25.7	32.7

A papain-solubilized form of the human class II MHC molecule, HLA-DR1 (DRA, DRB1*#0101*)[58] was co-crystallized with SEB in a 1:1 molar ratio (final total protein concentration, 15 mg ml^{-1}) from a stock solution in 10 mM Tris buffer, pH 7.5. Crystals were grown by vapour diffusion, by mixing 2 µl protein solution with 2 µl well solution containing 10 mM sodium acetate, pH 4.7, 10% ethylene glycol, and 12–20% PEG4000 (Fluka), at 25 °C. SEB was obtained as a lyophilized powder from Sigma, or Toxin Technology, from culture supernatants of an SEB-producing strain of *S. aureus* (Toxin Technology) and as a kind gift from M. Sax. Two crystal forms grew under the same conditions. Data for crystal form I were collected from crystals flash-frozen at −165 °C. Data for crystal form II were collected from 8 crystals at 25 °C and merged using the Buddha[59] and CCP4 programs[60]. Data were collected using a Nicolet/Xentronics area detector and Elliot GX-13 rotating-anode X-ray source with Franks double-mirror optics, and also at the Cornell High Energy Synchrotron Source (CHESS) F-1 beamline, using Kodak phosphor-image plates. CHESS data were processed with Denzo and Scalepack (Z. Otwinowski, personal communication). DR1–SEB SIR/anomalous phased electron density maps were iteratively averaged with DR1–SIR electron density maps and a model of the HLA-DR1 molecule was built as described[11]. The SEB region was not easily interpretable, so the DR1 model was improved, first by building into single DR1 domain omit maps, comparing maps calculated with both model and experimental SIR/anomalous phases, and maps calculated with DR1 model phases. Cycles of building and refinement of the DR1 model improved the SEB regions and a partial polyalanine model of SEB was built. This partial model of the DR1–SEB structure was used to solve the second, low-resolution DR1:SEB crystal form by molecular replacement using the Navazza suite of programs[61], giving an initial *R*-factor of 40.5% and a correlation coefficient of 48.4% from 8–4.3 Å. Iterative four-fold real-space averaging between the two space groups was carried out using the Bricogne package of programs[62], generating the electron density map shown in Fig. 1*a*. A 190-residue polyalanine trace of SEB was built and used to phase five higher-resolution (3.5 Å) maps, where 20% of the SEB polyalanine trace was omitted. Side chains were built into interpretable electron density, and the model was improved by further cycles of building, refinement and iterative two-fold non-crystallographic real-space averaging. The resolution was gradually extended from 3.5 to 2.7 Å. At all stages, refinement paths were taken that minimized the free *R*-factor[63]. As refinement proceeded, a number of loops in the SEB structure remained untraceable. These loops include residues 57–60 and 99–110 of the first domain and residues 122–126, 176–182, and the N- and C-terminal residues 1 and 236–239 of the second domain. In addition, three regions in the C-terminal domain of SEB do not show unambiguous side-chain density, including the N-terminal SEB region (residues 1–11) β-strands 6 and 7 (residues 127–154), and the C-terminal region of helix 4 and the adjacent loop residues (residues 169–175). In general, density for the second domain is less well defined. Refinement shows a dramatic difference in average atomic *B*-factor values between the HLA-DR1 molecule and the SEB molecule. The average Cα *B*-factor is 30 Å^2 for DR1, 55 Å^2 for the N-terminal domain of SEB1 (SEB1 is one of the SEB molecules in the asymmetric unit), and 70–80 Å^2 for the C-terminal domain, showing a radial increase from the DR1–SEB interface (Fig. 1). Given the high temperature factors for SEB, it was important to verify the SEB model. An independently refined model of HLA-DR1 (ref. 20), with no phase bias for the SEB model, was used to calculate $|2F_{obs} - F_{calc}|$ averaged and unaveraged omit maps. The omit maps verified the overall placement of the SEB molecule in the map, indicating a deteriorating map quality for SEB regions in the following order: N-terminal domain (SEB1) > C-terminal domain (SEB1) ~ N-terminal domain (SEB2) > C-terminal domain (SEB2), where SEB1 and SEB2 refer to the two SEB molecules in the asymmetric unit. In the final stages, the independently determined structure of the SEC3 molecule was compared to the SEB model, leading to rebuilding of difficult regions of the SEB, including three loops (29–32, 201–203 and 224–229), the N-terminal strand (residues 2–13), and the C-terminal residues of helix 4 and the adjacent loop (157–175). Fewer than 5% of the Φ/Ψ angles lie outside allowed regions of a Ramachandran plot.

* $R_{sym} = \sum |I - \langle I \rangle| / \sum I$, where I is the observed intensity, and $\langle I \rangle$ is the average intensity from several measurements.

† 9,400 non-hydrogen atoms represents 93% of the expected atoms for the DR1–SEB complex. Water molecules have not yet been included in this refinement.

‡ R.m.s. bond angles and lengths are r.m.s. deviations from ideal values.

§ *R*-factor calculated with working set reflections greater than 2σ.

‖ *R*-factor calculated with 3,383 reflections removed before automated refinement and greater than 2σ.

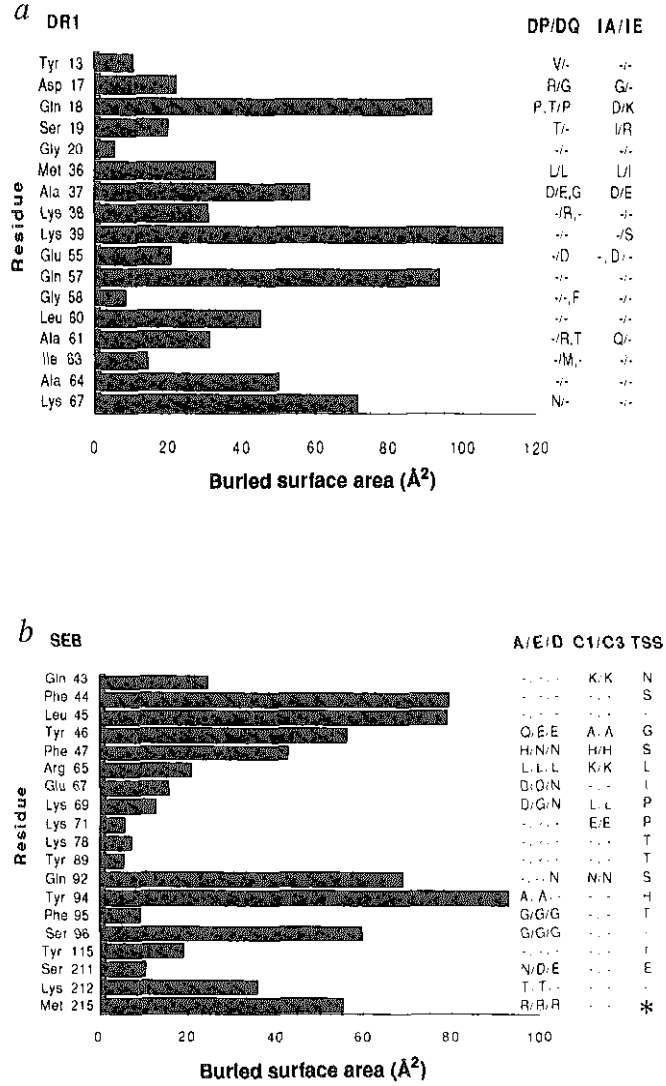

FIG. 5 Residues involved in the DR1–SEB interaction vary between class II isotypes and related superantigens. *a*, Plot of the buried solvent-accessible surface area[22] for each residue of the HLA-DR1 molecule involved in SEB binding. Corresponding residues in HLA-DP, HLA-DQ, mouse I-A, and I-E molecules is indicated to the right of the plot. *b*, Plot of the buried solvent-accessible surface area for each residue of the SEB molecule involved in HLA-DR1 binding. Corresponding residues in related superantigens are listed to the right for SEA, SED, SEE, SEC1, SEC3 and TSST-1. The TSST-1 residue alignment is based on the structural alignment of TSST-1 and SEB[38,39]. Surface areas were calculated with the program Access[22] as described in Fig. 4 legend. A dash is used for residues identical to DR1 or SEB and an asterisk indicates a deletion.

antigen stimulation through direct TCR–MHC interactions[16,24,26,29,46–53].

However, the DR1–SEB complex suggests that the interactions between TCR and MHC molecules during superantigen stimulation differ from the interactions involved in antigenic peptide stimulation. Residues of the DR1 α1-domain α-helix that are usually exposed and might interact with the TCR are partially or completely buried in the complex by SEB residues 92–96 (Fig. 3*c*). These MHC surface residues (at positions 55, 57, 58, 60, 61, 63, 64, 67) influence T-cell stimulation when mutated[12,13], indicating that this region of the DR α1-domain α-helix is important for TCR recognition of peptide antigens and arguing for an unconventional mode of interaction between TCR and MHC during superantigen stimulation.

Discussion

The crystal structure of the DR1–SEB complex shows that SEB binds to the α1 domain of class II molecules, positioning a TCR-binding site above and to the side of the MHC peptide-binding site. Antigenic peptides are not inhibitors of SEB stimulation[13] and the structure demonstrates that peptides and SEB occupy two distinct regions of the class II MHC molecule. In the DR1–SEB crystal, electron density is observed for 13 residues of an extended peptide chain, corresponding to a mixture of self peptides bound to DR1 (T.S.J., manuscript in preparation). The details of the DR1–SEB interaction indicate how superantigen affinity could be modulated for different class II isotypes.

The interaction of related bacterial superantigens with class II molecules may differ from that seen in the DR1–SEB structure. Two lines of evidence support such a view. The first is that different superantigens do not all cross-compete in binding studies. SEB and TSST-1 do not competitively inhibit each other or completely block SEA binding to HLA-DR[28,30,31], indicating the existence of independent binding sites. However, SEA is able to compete effectively with both SEB and TSST-1 for binding[31], suggesting that these sites may overlap. In addition, mutational studies of HLA-DR and SEA suggest that SEA has a different binding site. Histidine 81 of the class II β-chain[32,33] is important for SEA binding to DR, but has no effect on SEB or TSST-1 binding. This interaction may be mediated by a zinc atom bound to a metal coordination site found in SEA, SED and SEE[54]. SEB does not require zinc to bind class II molecules, and the residues in SEA that bind zinc are in the C-terminal domain, far from the DR1–SEB interface, indicating that SEA has a different mode of binding from SEB.

Important features of the DR1–SEB interaction are conserved in SEA, suggesting that SEA may have evolved two distinct modes of binding to class II molecules, one similar to SEB and another zinc-mediated interaction with the class II β-chain. This is consistent with the available mutational and binding data.

Binding of one SEA molecule to both α-chain and β-chain sites on one class II molecule is unlikely, considering the DR1–SEB structure, the competition data, and the zinc-binding site of SEA. However, one SEA molecule could potentially crosslink two class II molecules, with the N-terminal domain interacting with the α1 domain of class II (as observed for SEB) and the C-terminal domain interacting with the β-chain of another class II molecule. This type of crosslinking might explain the ability of these superantigens to stimulate T cells at concentrations well below their measured K_d values.

The crystal structure also supports a model of ternary complex formation in which the MHC interaction with the TCR is distinct from the peptide-mediated interaction. A stretch of residues located in the SEB disulphide loop lies across the α1 α-helix of DR1, covering residues that have been implicated in TCR recognition of peptide–MHC complexes. This suggests that superantigens may not take advantage of any residual affinity of TCR for MHC derived from positive selection during thymic education. However, the location of SEB residues that interact with TCR and of TCR residues that interact with superantigens suggests that the TCR may still be positioned in close proximity to the class II peptide-binding site. This may explain how TCR α-chains and MHC polymorphisms can modulate superantigen stimulation. Superantigens may have evolved to bind class II MHC molecules, not in order to use existing MHC–TCR interactions to stimulate T cells, but rather to take advantage of additional signals and organization inherent in conventional antigen presentation.

Superantigens have been directly implicated in a number of diseases and it has been suggested that they might be involved in the generation of autoimmunity[55] by stimulating existing autoreactive T cells. It has been shown that SEB can induce relapsing paralysis in mice that have previously been immunized with a peptide that induces experimental autoimmune encephalomyelitis[56,57]. This indicates that the powerful T-cell-activation properties of superantigens may be important in the development and relapse of autoimmune disorders. An understanding of the structural requirements for the action of these superantigens may further the development of strategies to control the onset and progression of disease. □

Received 14 February; accepted 31 March 1994.

1. Herman, A., Kappler, J. W., Marrack, P. & Pullen, A. M. *A. Rev. Immunol.* **9,** 745–772 (1991).
2. Irwin, M. J., Hudson, K. R., Ames, K. T., Fraser, J. D. & Gascoigne, N. R. J. *Immun. Rev.* **131,** 61–78 (1993).
3. Micusan, V. V. & Thibodeau, J. *Semin. Immun.* **5,** 3–11 (1993).
4. Marrack, P. *et al. Immun. Rev.* **131,** 79–92 (1993).
5. Marrack, P., Blackman, M., Kushnir, E. & Kappler, J. *J. exp. Med.* **171,** 455–464 (1990).
6. Miethke, T. *et al. J. exp. Med.* **175,** 91–98 (1992).
7. Kotzin, B. L., Leung, D. M., Kappler, J. & Marrack, P. *Adv. Immun.* **54,** 99–166 (1993).
8. Germain, R. M. & Margulies, D. H. *A. Rev. Immun.* **11,** 403–450 (1993).
9. Madden, D. R., Garboczi, D. N. & Wiley, D. C. *Cell* **75,** 693–708 (1993).
10. Matsumura, M., Fremont, D. H., Peterson, P. A. & Wilson, I. A. *Science* **257,** 927–934 (1992).
11. Brown, J. H. *et al. Nature* **364,** 33–39 (1993).
12. Jorgensen, J. L., Reay, P. A., Ehrich, E. W. & Davis, M. M. *A. Rev. Immun.* **10,** 835–873 (1992).
13. Dellabona, P. *et al. Cell* **62,** 1115–1121 (1990).
14. Choi, Y. *et al. Nature* **346,** 471–473 (1990).
15. Cazenave, P. A. *et al. Cell* **63,** 717–728 (1990).
16. Pullen, A. M., Wade, T., Marrack, P. & Kappler, J. W. *Cell* **61,** 1365–1374 (1990).
17. Pullen, A. M., Bill, J., Kubo, R. T., Marrack, P. & Kappler, J. W. *J. exp. Med.* **173,** 1183–1192 (1991).
18. White, J., Pullen, A., Choi, K., Marrack, P. & Kappler, J. W. *J. exp. Med.* **177,** 119–125 (1993).
19. Swaminathan, S., Furey, W., Pletcher, J. & Sax, M. *Nature* **359,** 801–806 (1992).
20. Stern, L. J. *et al. Nature* **368,** 215–221 (1994).
21. Buelow, R. *et al. J. Immun.* **148,** 1–6 (1992).
22. Lee, B. & Richards, F. M. *J. molec. Biol.* **55,** 379–400 (1971).
23. Connolly, M. L. *J. appl. Crystallogr.* **16,** 548–558 (1983).
24. Kappler, J. W., Herman, A., Clements, J. & Marrack, P. *J. exp. Med.* **175,** 387–396 (1992).
25. Scholl, P. R. *et al. J. Immun.* **144,** 226–230 (1990).
26. Herman, A., Croteau, G., Sekaly, R. P., Kappler, J. & Marrack, P. *J. exp. Med.* **172,** 709–717 (1990).
27. Herrmann, T., Accolla, R. S. & MacDonald, H. R. *Eur. J. Immun.* **19,** 2171–2174 (1989).
28. Fraser, J. D. *Nature* **339,** 221–223 (1989).
29. Mollick, J. A., Chintagumpala, M., Cook, R. G. & Rich, R. R. *J. Immun.* **146,** 463–468 (1991).
30. Scholl, P. R., Diez, A. & Geha, R. S. *J. Immun.* **143,** 2583–2588 (1989).
31. Chintagumpala, M. M., Mollick, J. A. & Rich, R. R. *J. Immun.* **147,** 3876–3881 (1991).
32. Herman, A. *et al. Proc. natn. Acad. Sci. U.S.A.* **88,** 9954–9958 (1991).
33. Karp, D. R. & Long, E. O. *J. exp. Med.* **175,** 415–424 (1992).
34. Karp, D. R., Teletski, C. L., Scholl, P., Geha, R. & Long, E. O. *Nature* **346,** 474–476 (1990).
35. Panina-Bordignon, P., Fu, X.-t., Lanzavecchia, A. & Karr, R. W. *J. exp. Med.* **176,** 1779–1784 (1992).
36. Braunstein, N. S., Weber, D. A., Wang, X. C., Long, E. O. & Karp, D. *J. exp. Med.* **175,** 1301–1305 (1992).
37. Harris, T. O. *et al. Infect. Immun.* **61,** 3175–3183 (1993).
38. Prasad, G. S. *et al. Biochemistry* **32,** 13761 13766 (1993).
39. Acharya, K. R. *et al. Nature* **367,** 94–97 (1994).
40. Thibodeau, J., Labreque, N., Denis, F., Huber, B. & Sékaly, R.-P. *J. exp. Med.* **179,** 1029–1034 (1994).
41. Hudson, K. R., Robinson, H. & Fraser, J. D. *J. exp. Med.* **177,** 175–184 (1993).
42. Mollick, J. A., McMasters, R. L., Grossman, D. & Rich, R. R. *J. exp. Med.* **177,** 283–293 (1993).
43. Grossman, D., Van, M., Mollick, J. A., Highlander, S. K. & Rich, R. R. *J. Immun.* **147,** 3274–3281 (1991).
44. Chothia, C., Boswell, D. R. & Lesk, A. M. *EMBO J.* **7,** 3745–3755 (1988).
45. Gascoigne, N. R. J. & Ames, K. T. *Proc. natn. Acad. Sci. U.S.A.* **88,** 613–616 (1991).
46. Yagi, J., Rath, S. & Janeway, C. A. Jr *J. Immun.* **147,** 1398–1405 (1991).
47. Herrmann, T., Maryanski, J. L., Romero, P., Fleischer, B. & MacDonald, H. R. *J. Immun.* **144,** 1181–1186 (1990).
48. Smith, H. P., Le, P., Woodland, D. L. & Blackman, M. A. *J. Immun.* **149,** 887–896 (1992).
49. Vacchio, M. S., Kanagawa, O., Tomonari, K. & Hodes, R. J. *J. exp. Med.* **175,** 1405–1408 (1992).
50. Blackman, M. A., Smith, H. P., Le, P. & Woodland, D. L. *J. Immun.* **151,** 556–565 (1993).
51. Gascoigne, N. R. J. *Semin. Immun.* **5,** 13–21 (1993).
52. Waanders, G. A., Lussowe, A. R. & MacDonald, H. R. *Int. Immun.* **5,** 55–61 (1993).
53. Woodland, D. L. *et al. J. exp. Med.* **177,** 433–442 (1993).
54. Fraser, J. D. & Hudson, K. R. *Res. Immun.* **144,** 188–193 (1993).
55. Paliard, X. *et al. Science* **253,** 325–329 (1991).
56. Brocke, S. *et al. Nature* **365,** 642–644 (1993).
57. Soos, J., Schiffenbacher, J., Wegrzyn, L. & Johnson, H. M. *J. Immun.* **150,** 192A (1993).
58. Gorga, J. C., Horejsi, V., Johnson, D. R., Raghupathy, R. & Strominger, J. L. *J. biol. Chem.* **262,** 16087–16094 (1987).
59. Blum, M., Metcalf, P., Harrison, S. C. & Wiley, D. C. *J. appl. Crystallogr.* **20,** 235–242 (1987).
60. *CCP4: A Suite of Programs for Protein Crystallography* (SERC Collaborative Computing Project No. 4, Daresbury Laboratory, Warrington, UK, 1979).
61. Navaza, J. *Acta crystallogr.* **A43,** 645–653 (1987).
62. Bricogne, G. *Acta crystallogr.* **A32,** 832–847 (1976).
63. Brünger, A. T. *Nature* **355,** 472–475 (1992).
64. Jones, T. A., Zou, J.-Y., Cowan, S. W. & Kjeldgaard, M. *Acta crystallogr.* **A47,** 110–119 (1991).
65. Kraulis, P. J. *J. appl. Crystallogr.* **24,** 945–949 (1991).

ACKNOWLEDGEMENTS. We thank P. Rosenthal, S. Garman, M. Eisen and staff of the Cornell High Energy Synchrotron Source MacCHESS for help with data collection, P. Klimotovsky and A. Haykov for additional technical assistance; and M. Blum and other members of our groups for discussion. T.S.J. was supported by the Cancer Research Institute; J.H.B. by the Howard Hughes Medical Institute (HHMI); J.C.G. by the Juvenile Diabetes Foundation International; L.J.S. by a Damyon Runyon–Walter Winchell Cancer Fellowship and HHMI; R.G.U. by the Irvington Institute; Y.I.C. and C.U.S. by the Lucille P. Markey Foundation Trust; and J.L.S. by the NIH, D.C.W. is an investigator with the Howard Hughes Medical Institute. Coordinates will be deposited in the Brookhaven Protein Databank and are available from the authors.